Pergamon

Journal of Structural Geology, Vol. 17, No. 5, pp. 727 to 738, 1995
Elsevier Science Ltd
Printed in Great Britain

0191-8141(94)00095-6

The effects of rheology on the strain distribution in single layer buckle folds

LABAO LAN and PETER J. HUDLESTON

Department of Geology and Geophysics, University of Minnesota, Minneapolis, MN 55455, U.S.A.

(*Received* 28 *March* 1994; *accepted in revised form* 18 *August* 1994)

Abstract—Folds in rock provide opportunities for establishing how fabric and deformation mechanisms vary with local variations in strain and strain rate, and strain distribution in folds should, in principle, provide information on rheological conditions during folding. To investigate this, we use finite element models to simulate buckling in single-layer folds in incompressible, power-law materials in plane strain. Numerical results show that the pattern of strain variation in buckle folds is sensitive to variations in the power-law exponent, n_L, of the stiff layer. For a given amplitude, wavelength/thickness, and ratio of viscosities, m, of layer to matrix, strain and strain gradient along the axial trace increase more rapidly away from the neutral surface (on both sides) for power-law ($n_L > 1$) materials than for Newtonian ($n_L = 1$) materials.

Buckling strain is superimposed on early uniform layer-parallel shortening, which becomes greater as initial amplitude decreases and as n_L and m decrease. The effect of this superposition can best be described by reference to the infinitesimal neural surface (INS) and finite neutral surface (FNS), which vary in position with degree of overall shortening. The INS and FNS move from the outer arc towards the inner arc during buckling, the latter following the former. Thus, at any stage of folding, the layer can be divided into three zones with different coaxial, non-linear strain histories. Fabric in natural folds is expected to reflect such unsteady flow conditions.

INTRODUCTION

Folding in rocks and other layered materials is accompanied by distortions or strains within the layers. The pattern of these strains is characteristic of the folding mechanism, and the patterns can be studied directly in natural folds and by using both analog models and numerical models (Biot *et al.* 1961, Ramberg 1963a,b, Ghosh 1966, 1968, Chapple 1968, Dieterich & Carter 1969, Hobbs 1971, Hudleston 1973, Shimamoto & Hara 1976). In isotropic homogeneous materials, the strain pattern in stiff folded layers is typically one of layer-parallel stretching in the outer arc and layer-parallel shortening in the inner arc—a pattern known as *concentric-longitudinal strain* (Ramberg 1961) or *tangential-longitudinal strain* (Ramsay 1967, pp. 397–400). A neutral surface, connecting points of no strain, exists between the zones of extensional and contractional strains (Fig. 1a). In viscous or plastic materials, tangential-longitudinal strain may be superimposed on earlier homogeneous strains, in which case the strain pattern may be more complex and a neutral surface may not exist (Fig. 1b) (Hudleston & Holst 1984, Hudleston & Tabor 1988). In multilayered or strongly anisotropic rocks, layer-parallel shear may dominate the strain pattern, in a process known as *flexural slip* or *flexural flow* (Donath & Parker 1964, Ramsay 1967, pp. 391–396).

We focus our attention in this paper on the strain patterns in buckle folds developed in isolated stiff isotropic viscous layers. Previous studies of progressive buckle fold development in such layers have shown that the history of deformation is quite complicated and that fold development is accompanied by continuous changes in the states of stress and strain throughout the layer and the adjacent matrix (e.g. Chapple 1968, Dieterich & Carter 1969, Dieterich 1970). One of the principal aims of the present paper is to demonstrate how the strain pattern in the stiff layer and the evolution of this pattern with fold growth are dependent on the rheological properties of the layer. The information so obtained may be of help in the interpretation of strain patterns in natural folds in terms of the rheological state of the rocks during folding. Natural folds in stiff layers isolated from their neighbors within a homogeneous softer matrix are not common, but we believe they exist in sufficient quantity to enable systematic study for this purpose to be made. Earlier studies of natural single-layer folds, focusing on wavelength/thickness characteristics, include those of Sherwin & Chapple (1968), Hudleston & Holst (1984) and Holst (1987).

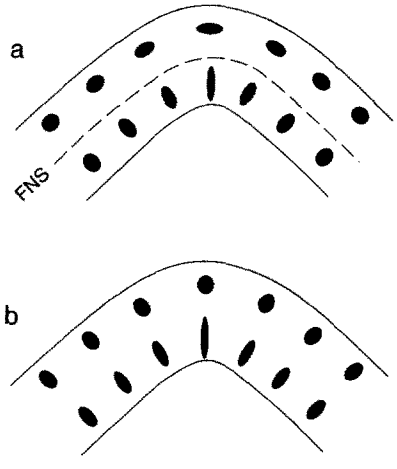

Fig. 1. Schematic strain patterns in the hinge regions of folds. (a) Buckling only: layer-parallel stretching in the outer arc and layer-parallel shortening in the inner arc, FNS—finite neutral surface. (b) Uniform strain preceding buckling: contractional strain everywhere, no finite neutral surface.

We have shown, in earlier papers on fold shape (Hudleston & Lan 1993, 1994) that, given suitable circumstances, curvature of single-layer buckle folds, can be used to get some idea of the degree of non-linearity of the flow law. Clearly, there is some relationship between the shapes of the bounding surfaces of a folded layer and the strain distribution within the layer, and so we would expect the two to show sympathetic dependencies on rheological parameters.

In many instances strain cannot be measured in rocks directly, but mineral fabrics (crystallographic preferred orientations and shape preferred orientations) have the potential to reflect strain and strain history (Lister 1977, Simpson & Schmid 1983, Law 1990), and folds provide ideal settings in which to study natural variations in fabric with strain and strain history, under conditions of constant temperature and initial lithology. For many years, fabric analysis and the determination of finite strain associated with folding have been used to help understand folding processes and to assist in reconstructing the history of deformation (e.g. Cloos 1947, Ramsay 1967, Groshong 1975, Pfiffner 1980, Hudleston & Holst 1984, Hudleston & Tabor 1988). An analysis of strain development with fold growth in analog or numerical models allows strain histories at different parts of a fold to be tracked. A second objective of this paper is to provide a detailed account of strain development in buckle folds that may help in the analysis of natural fabric variations.

Our knowledge of the likely form of the constitutive relationships appropriate for rock deforming under natural conditions comes from laboratory experiments, extrapolated with some uncertainty to the much slower strain rates occurring in nature (Paterson 1987). Diffusive deformation mechanisms give rise to linear flow laws (e.g. Elliott 1972, Nicolas & Poirier 1976) and creep involving dislocation movement, likely to be important in much of the ductile part of the crust on the basis of much experimental work (e.g. Carter 1976, Kirby & Kronenberg 1987), gives rise to a power-law constitutive relationship, with values of the power-law exponent typically in the range of 2–8.

We use in this paper a finite element code that incorporates a power-law constitutive relationship of the kind appropriate for simulating Newtonian (linear) or power-law viscous flow of rocks, and we apply this to study the development of strain in symmetrical single-layer buckle folds. We are particularly interested in seeing how the strain distribution varies as a function of the power-law exponent, n_L, of the stiff layer and in seeing, for different values of n_L and of the ratio of viscosities of layer to viscosity of matrix, how the neutral surface develops and migrates during fold growth.

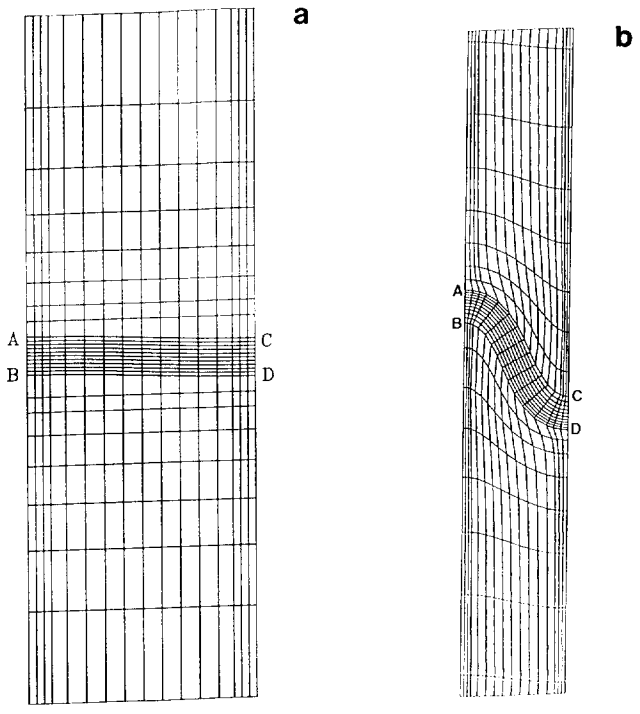

Fig. 2. (a) Initial finite element grid (one half wavelength) for strain analysis. ABCD represents the stiff layer. A small sinusoidal perturbation (initial amplitude/thickness, $A_o/h_o = 0.1$) is imposed on the layer before deformation. For boundary conditions, see Lan & Hudleston (1991, fig. 1). (b) Deformed configuration from (a) for $L_o/h_o = 12$, $n_L = 3$, $n_M = 1$ and $m = 215$, after 40% layer-parallel shortening.

NUMERICAL MODELS

The finite element code used in this study is based on one developed by Hanson (1990) for simulating flow of glaciers. We have described the basic application of this code to problems of folding in earlier papers (Lan & Hudleston 1991, Hudleston & Lan 1994). We will simply note here that fold growth is studied by solving a series of quasi steady-state problems, with time steps sufficiently small to allow the exponential growth of the fold to be tracked accurately. There is one difference between the models described in this paper and the earlier models, and that is in the number of elements employed. To improve the accuracy and resolution of strain in the stiff layer, 160 elements (in one half wavelength, see Fig. 2a) are used, rather than 48 as in the earlier models. In the text, the subscripts L and M refer to layer and matrix, respectively, and the subscript o refers to the initial state. 'Wavelength' (measured along the fold arc) and thickness at any stage during deformation are represented by L and h, respectively. The initial thickness of the stiff layer parallel to the axial trace is h_o, and this is also very nearly equal to the initial orthogonal thickness throughout the fold (see Fletcher 1979). The thickness, h, at any deformational stage is an average orthogonal thickness calculated by $h = L_o h_o / L$ (given constant volume). All folds produced in our models are class IB (parallel) or deviate slightly from IB in the field of class IC (cf. Hudleston & Lan 1994, figs. 12 and 13). The percentage bulk shortening in the direction parallel to the layer is termed S.

As in the previous studies (Lan & Hudleston 1991, Hudleston & Lan 1994) the initial perturbations were sinusoidal in form, and models were made employing two initial geometries (three with initial wavelength/thickness, $L_o/h_o = 12$, initial amplitude/thickness, A_o/h_o

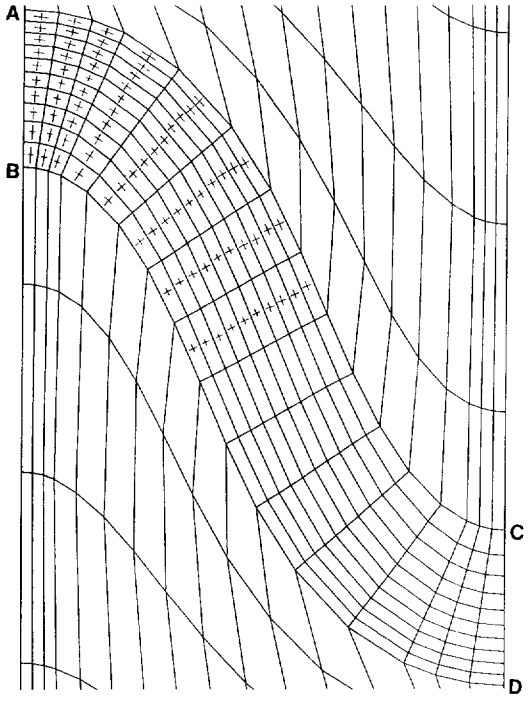

Fig. 3. Part of Fig. 2(b) enlarged with principal strains shown. The short orthogonal lines in the center of each element represent the magnitudes and orientations of the principal finite strains.

= 0.1, and three with $L_o/h_o = 20$, $A_o/h_o = 0.167$). In all models, the viscosity ratio ($\mu_L/\mu_M = m$ = viscosity layer/viscosity matrix) for the basic flow was given values m = 10, 215 and 630 for power-law exponent of the stiff layer, $n_L = 1$, 3 and 10, respectively, for each of the two starting configurations. In addition, a set of models was run with all parameters fixed ($A_o/h_o = 0.1$, $L_o/h_o = 12$, $m = 100$) except the power-law exponent of the layer, which was given the values $n_L = 1$, 3 and 10. These combinations of parameters lie in the range of what might be expected under natural conditions. Further discussion of the choice of parameters is given in Hudleston & Lan (1994).

Fletcher (1974) has shown that the power-law exponent of the matrix has a small effect on the buckling instability, when the rheological parameters are appropriately expressed, and so to save computational time the matrix material was made linear viscous ($n_M = 1$) in all models.

All calculations were performed on Cray-2 and Cray C90 supercomputers. Figures 2(b) and 3 show the element grid in the deformed state and the magnitudes and orientations of principal cumulative strain, after 40% shortening, for a selected set of rheological parameters. To follow a common convention in geological discussions of strain, the expression 'finite strain' is used in this paper to denote the total strain accumulated at any stage of the deformation.

RESULTS

Effects of layer-parallel shortening

Buckle folding in viscous materials is accompanied in its early stages by layer-parallel shortening, which results in a nearly homogeneous strain of the whole system, while the fold amplitudes remain small (limb dips ≤ 10–15°). The incremental 'shortening' strain in the stiff layer diminishes in magnitude and becomes heterogeneous as the fold grows. We discuss first the effects of such layer-parallel shortening, before we consider the strain due to buckle folding.

A simple way to record the overall shortening of the layer is to plot the ratio of arclength to initial arclength, L/L_o, or (arclength/thickness)/(initial arclength/initial thickness), $(L/h)/(L_o/h_o)$, as a function of bulk shortening, S (Fig. 4). Because $L = L_o\sqrt{\lambda_2}$ and $h = h_o\sqrt{\lambda_1}$ for a flat layer, the quantity $(L/h)/(L_o/h_o)$ is equal to the homogeneous strain, $\sqrt{\lambda_2}/\sqrt{\lambda_1}$, experienced by the layer and the whole rock, where λ_1 and λ_2 are the principal quadratic elongations. As the fold grows, these quantities will cease to track the bulk strain. If the layer folds without any change in length or thickness, $L/L_o = (L/h)/(L_o/h_o) = 1$.

We can see from Fig. 4 that layer-parallel shortening occurs in all cases, and that the amount of such shortening depends strongly on n_L and m. The higher the value of n_L or m, the smaller the amount of shortening. For n_L = 3 and 10, shortening is modest and occurs mostly during the early stages of deformation. The total 'homogeneous' shortening experienced by the layer is less than 3% ($\sqrt{\lambda_2}/\sqrt{\lambda_1} = (L/h)/(L_o/h_o) \geq 0.94$) for $L_o/h_o = 20$ and n_L = 3 or 10, less than 8% ($\sqrt{\lambda_2}/\sqrt{\lambda_1} \geq 0.85$) for L_o/h_o = 12 and n_L = 3, and less than 5% ($\sqrt{\lambda_2}/\sqrt{\lambda_1} \geq 0.90$) for L_o/h_o = 12 and n_L = 10, as can be seen in Figs. 4(a) & (b) (with m = 215 for n_L = 3 and m = 630 for n_L = 10). For m = 100 and L_o/h_o = 12 (Fig. 4c), the shortening is similar for all three values of n_L, but greatest for n_L = 1 and least for n_L = 10. Maximum shortening is about 12% for n_L = 1, and 11% for n_L = 3 and 10. For n_L = 1 and m = 10, layer-parallel shortening is much more pronounced, and in fact closely tracks the curve representing bulk homogeneous strain until a shortening, S, of ca. 30%, for both L_o/h_o = 12 and L_o/h_o = 20 (Figs. 4a & b). The slight increase in $(L/h)/(L_o/h_o)$ at values of shortening above 50% (see Figs. 4a & b) is due to elongation of the limbs as they rotate into positions of extensional strain.

Strain history at selected locations around the folds

It is instructive to consider the development of strain at selected locations around folds developed from the same initial configuration, differing in the values of n_L and m. We select three locations, corresponding to elements in the outer and inner arcs of the hinge and at the middle of the layer at the inflexion point, and compare the results for the three models with L_o/h_o = 12, n_L = 1, 3 and 10, and m = 10, 215 and 630, respectively (Fig. 5). In the inner arc of the fold (element 213), strain is compressive (λ_1 vertical—indicated by positive values in the figure) along the layering, throughout fold growth, in all three cases (n_L = 1, 3, 10), strain magnitude increasing monotonically with shortening (Fig. 5b). The greatest strain attained (by 60% shorten-

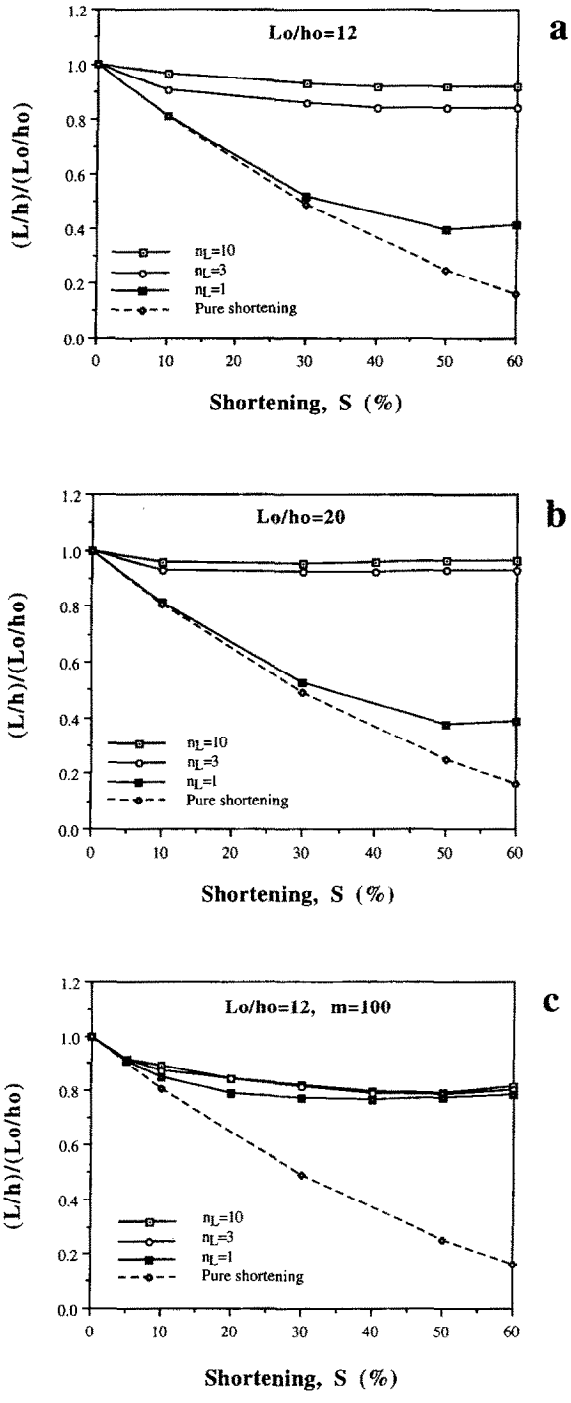

Fig. 4. Variation of wavelength/thickness (L/h), in terms of initial wavelength/thickness (L_o/h_o), with shortening, S (%). Dashed lines show pure shortening (bulk strain)—passive deformation. (a) For m = 10, 215 and 630, and n_L = 1, 3 and 10, L_o/h_o = 12. (b) For m = 10, 215 and 630, and n_L = 1, 3 and 10, L_o/h_o = 20. (c) For m = 100, L_o/h_o = 12 and n_L = 1, 3 and 10.

ing) is for $n_L = 1$, although until 30% shortening this location records the least strain when $n_L = 1$. In the outer arc of the fold (element 9) the situation is complicated by initial layer-parallel shortening, which opposes the extensional strain (λ_1 horizontal—indicated by negative values in the figure) due to buckling. In this case the strains in all three cases are initially compressional, becoming extensional at different amounts of bulk shortening ($S = 4\%$ for $n_L = 3$ and $S = 1\%$ for $n_L = 10$), when the buckling strain in the outer arc first exceeds the layer-parallel shortening (Fig. 5a). For $n_L = 1$ this never happens, and the maximum finite compressive strain remains parallel to the layer throughout fold development. We will return later in the paper to details of this history when we remove the effects of layer-parallel strain and consider the behavior of the neutral surface.

At the inflexion point (element 104), strains remain very small throughout the history of fold growth, for n_L = 3 and 10, with a maximum elongation perpendicular to the layer (Fig. 5c). This small strain is the 'locked in' early layer-parallel shortening. For $n_L = 1$ there is progressive development of strain during fold growth, associated with progressive layer shortening and thickening which is pronounced in this case (see Fig. 4).

Finite strain variations along the axial surface trace from outer arc to inner arc

Let us now consider how the strain varies along the axial trace, from outer arc to inner arc, at some fixed value of bulk shortening. This is the kind of data that might be obtained from natural folds. We represent the data in various ways. First, in Fig. 6(a) we plot the axial ratio of the finite strain ($\sqrt{\lambda_1}/\sqrt{\lambda_2}$) as a function of distance along the axial surface trace for the three models with the same initial geometry ($L_o/h_o = 12$) and same bulk shortening $S = 40\%$, and with m = 10, 215 and 630 for n_L = 1, 3 and 10, respectively. Note that the strain ratios in both inner and outer arcs for $n_L = 10$ are greater than those in equivalent positions for $n_L = 3$ (Fig. 6a), the two folds being otherwise of very similar amplitude and maximum limb dip. By plotting ($\sqrt{\lambda_1}/\sqrt{\lambda_2}$) as the ordinate in Fig. 6(a) we obscure the fact that layer-parallel strains in the outer arc for $n_L = 3$ and 10 are extensional and contractional in the inner arc, but emphasize the difference in strain magnitude between inner and outer arcs. The diminishing strain magnitude towards the center of the layer from both margins, however, indicates the approach to the neutral surface, which separates extensional from contractional strains. A discussion of strain gradients is more easily done if we plot the natural logarithm of the strain ratio against distance along the axial trace and record outer arc strains as positive ($R = \sqrt{\lambda_1}/\sqrt{\lambda_2}$; $\ln R = \ln\sqrt{\lambda_1} - \ln\sqrt{\lambda_2}$) and inner arc strains as negative ($R = \sqrt{\lambda_2}/\sqrt{\lambda_1}$; $\ln R = \ln\sqrt{\lambda_2} - \ln\sqrt{\lambda_1}$). This is done in Fig. 6(b), in which the position of the neutral surface is clear for n_L = 3 and 10. It is apparent in both Figs. 6(a) & (b) that there is no neutral surface for the case $n_L = 1$, and strains increase monotonically from outer arc to inner arc. This is because the buckling strains are superimposed on the early layer-parallel shortening, which is greater in magnitude than the largest extensional component of strain in the outer arc due to buckling.

It is clear in Fig. 6(b) that the gradient in strain along the axial trace increases from outer arc to inner arc in all three cases and is greatest for $n_L = 10$ and least for n_L = 1. These models, however, differ in their values of m, and we wish to consider the effect of varying n_L alone. In Fig. 7(a) we plot results for three models with the same

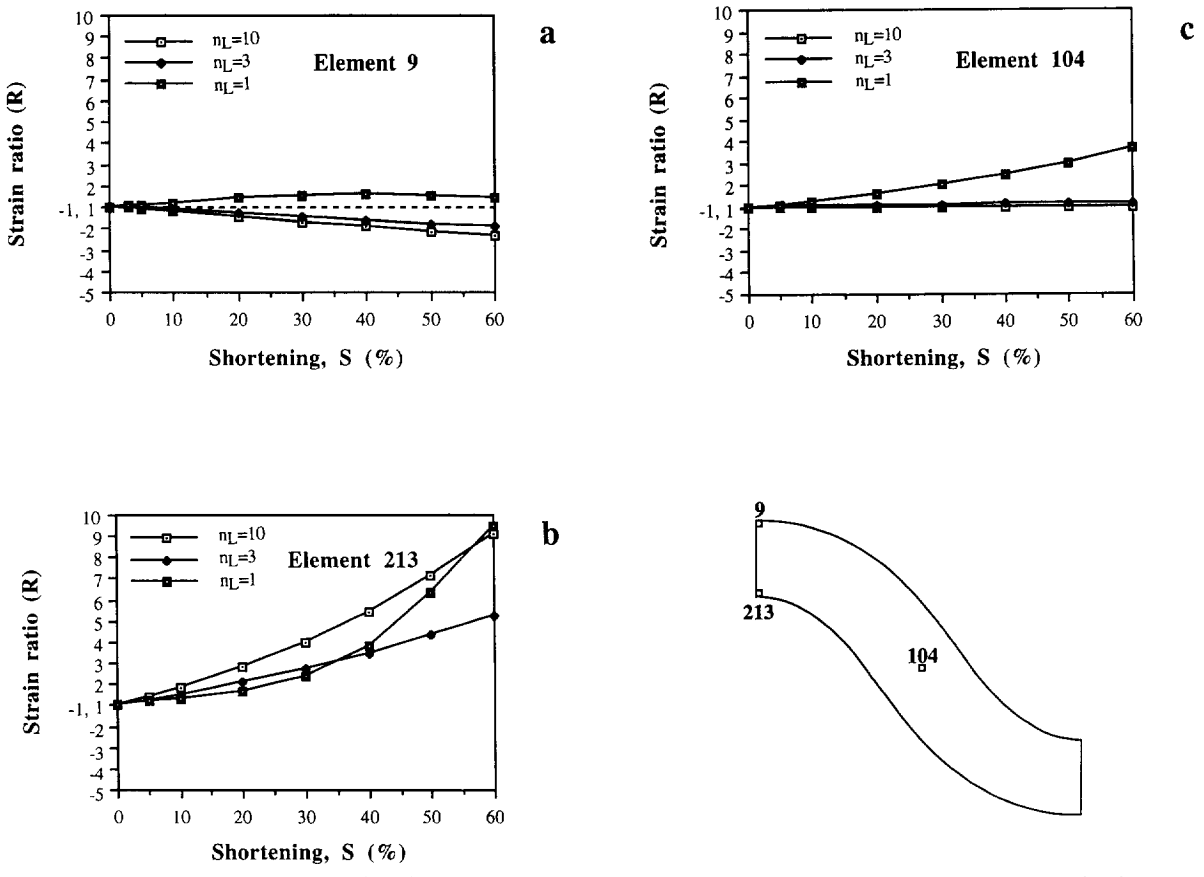

Fig. 5. Variation of strain ($R = \sqrt{\lambda_1}/\sqrt{\lambda_2}$) as a function of shortening, S, at selected locations in the folded layer for three models with different values of power-law exponent, n_L, of the stiff layer. Geometric and rheologic parameters are the same as those in Figs. 2 and 4. For λ_1 normal to the layer, strains are given as positive; for λ_1 parallel to the layer, strains are given as negative. (a) Outer arc at the fold hinge (element 9). Dashed lines represent the strain ratio, $R = 1.0$. (b) Inner arc at the fold hinge (element 213). (c) Limb in the middle of the layer (element 104). The inset shows the element locations.

value of viscosity ratio ($m = 100$) and $n_L = 1$, 3 and 10. We note the same dependence of strain gradient on n_L as is apparent in Fig. 6(b): the larger the value of n_L, the higher the gradient. We also note that, in this case, there now exists a neutral surface for $n_L = 1$. In general our results show that for a given L_o/h_o and fold amplitude, strain gradient along the axial trace depends more strongly on n_L than on m. This is consistent with our earlier findings on fold shape (Hudleston & Lan 1994).

All the strain profiles along the axial trace considered so far have used a Lagrangian frame of reference, with positions of elements referred to the undeformed grid, as in Fig. 2(a). An Eulerian frame of reference, with positions of elements referred to the deformed grid, as in Fig. 2(b), is more practical in studies of natural folds, and the data of Fig. 7(a) are presented in such a reference frame in Fig. 7(b). The strain profiles in all three cases are less non-linear (i.e. there is less variation in the derivative of the functions in Fig. 7) in the Eulerian representation. It is also apparent in Fig. 7(b) that the gradient is close to being linear in the outer part of the fold for $n_L = 1$, as predicted in the simple models of beam buckling or bending, and is more markedly non-linear for $n_L = 3$ and 10.

It is interesting to note that the strain curves for the three models intersect almost at the same point, which lies at the center of the layer in the undeformed grid and at the neutral surface in the deformed grid.

Removal of uniform shortening

The amount of layer-parallel shortening depends on the initial flatness of the layer as well as on viscosity ratio and the power-law exponent of the stiff layer. It is useful, therefore, to remove the shortening so that the strain due to buckling alone can be compared. It is actually not necessary to remove shortening to compare strain gradients, as was done in the previous section, because addition or removal of a uniform strain on Fig. 6(b) simply moves the plot vertically up or down. If strain due to buckling at any position, d, along the axial trace is $B = \sqrt{\lambda_1}/\sqrt{\lambda_2} = f(d)$, addition of a uniform strain, T, prior to buckling gives as the total strain $R = BT$, or $\ln R = \ln B + \ln T$.

One simple and approximate way to remove the effects of layer-parallel shortening is to assume that the finite neutral surface (FNS) due to buckling is located at the instantaneous middle of the layer throughout deformation (i.e. it is a non-material surface). Hudleston & Tabor (1988) showed this would be the case if strain accumulated plastically and work done in folding the layer was minimized. The axial ratio (T) of maximum to

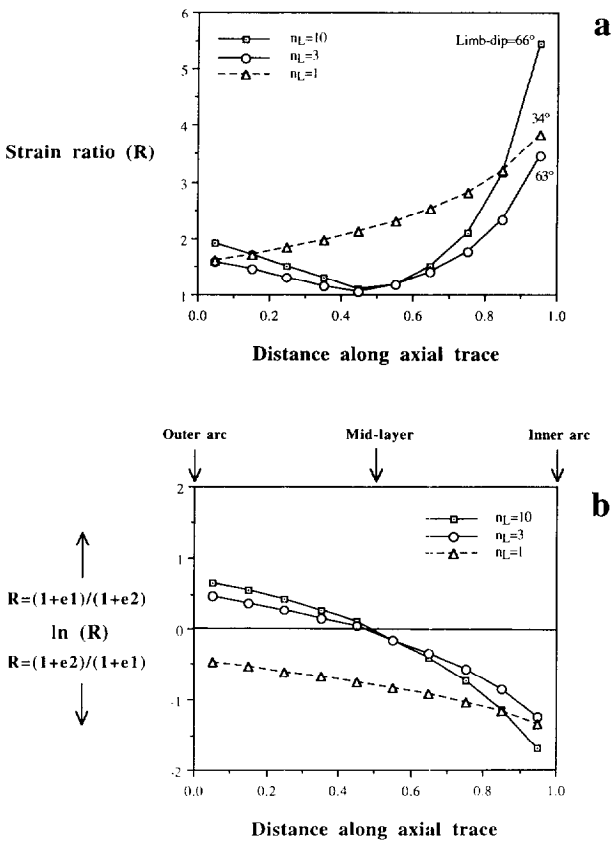

Fig. 6. Strain variation across the stiff layer in the fold hinge from outer arc to inner arc, with reference to the unstrained state. (a) Finite strain ratio, $R = (1 + e_1)/(1 + e_2)$, and (b) natural logarithm of finite strain ratio, $R = (1 + e_1)/(1 + e_2)$ or $(1 + e_2)/(1 + e_1)$, plotted against distance along the axial trace for $L_o/h_o = 12$, $m = 10$, 215 and 630, and $n_L = 1$, 3 and 10, after 40% shortening. Maximum limb dip shown for each model in (a). $(1 + e_1)$ and $(1 + e_2)$ are the maximum and minimum principal stretches. Dashed lines represent the linear model with $n_L = 1$.

minimum principal stretches of the homogeneous strain is then found in the following way. The strain ratio, T_m, at the center of the layer along the axial surface trace at any stage is found by interpolation of the numerical results. Assuming that the FNS lies at the center of the layer, the strain ratio due to buckle folding alone at this position must be unity. The interpolated value of T_m is thus equal to the layer-parallel shortening. The strain ratio $R = \sqrt{\lambda_1}/\sqrt{\lambda_2}$ at each point along the axial surface trace is the multiplied or divided by T_m according to whether the total layer-parallel strains are extensional or contractional. This gives the strains due to buckling. The curves in plots of the types shown in Figs. 6(b) or 7(a),(b) are then shifted up by an amount equal to ln T_m.

The argument that the neutral surface should lie at the middle of the layer does not hold for non-linear materials, because work done is no longer proportional to strain intensity (Hudleston & Tabor 1988). In this case, a more accurate method of removing the effects of layer-parallel shortening is to use the overall change in arclength and thickness during deformation and fold growth. We measure arclength from hinge to hinge along either bounding surface of the stiff layer at each stage of fold development. Average thickness at each stage can then be found from the condition that area is constant. The average axial ratio of the layer-parallel shortening strain is then given by $T_m = (h/h_o)/(L/L_o)$ or $(1/T_m) = (L/h)/(L_o/h_o)$. This is, in fact, what was plotted in Fig. 4, which displays the variation of average layer-parallel shortening strain, T_m, with bulk shortening, S. T_m at any stage is the strain at the FNS (for buckling alone). Values of strain along the axial surface can be corrected for layer-parallel shortening in the same way as for the first method. In the second method, however, the position of the FNS is not prejudged. As we will see later, the two methods do not in general give the same results.

Strain ratios along the axial surface trace of the folds for both linear and non-linear materials for the cases shown in Fig. 6(b), after removing the effect of uniform shortening, using the second method just described, are plotted in Fig. 8. The plots for $n_L = 3$ and 10 do not change much in position, but that for $n_L = 1$ changes substantially. We may see clearly from Fig. 8 that the value of the axial ratio of the strain due to buckling at equivalent positions along the axial surface trace of the fold, from outer arc to inner arc, increases as the power-law exponent, n_L, increases. This is consistent with the data for constant m (Fig. 7), in which the correction for removal of the uniform shortening is not necessary, because it is almost the same for all three cases (see Fig. 4c): thus all three curves in Fig. 7(a) or (b) would be shifted by about the same amount ($T_m \approx 1.26 - 1.30$).

We can also see from Fig. 8 that in any given fold the finite strain due to (buckling only) extension in the outer arc is always less than the finite strain due to (buckling only) contraction in the inner arc. Comparing Fig. 8 with Fig. 6(b), we can see the effect of removing the shortening strain—the plot just vertically moves up—mentioned above. With layer-parallel shortening removed, a finite neutral surface, of course, exists in all cases. It is clear that the position of the finite neutral surface on this plot shifts to the right along the horizontal axis, from the outer arc towards inner arc (compare Figs. 6b and 8), when layer-parallel shortening is removed.

The behavior of the infinitesimal neutral surface (INS) and finite neutral surface (FNS) during fold growth

We noted above that, at 40% bulk shortening in models developed from the same initial configuration but with different rheological properties, a finite neutral surface (FNS) exists in folds for $n_L = 3$ and 10 (and for $m = 215$ and 630, respectively), but not in the fold for $n_L = 1$ (and for $m = 10$) (Fig. 6). This difference in behavior is due to differences in the amount of layer-parallel shortening experienced in the three models. The strains due to buckling are superimposed on those due to layer-parallel shortening, the amount of which increases as viscosity ratio, m, power-law exponent, n_L, and initial amplitude, A_o, decrease. The effect of this superposition can best be described by reference to the neutral surface, and in this section we explore further the development of the neutral surface during fold growth.

First, it should be clear that there will in general exist

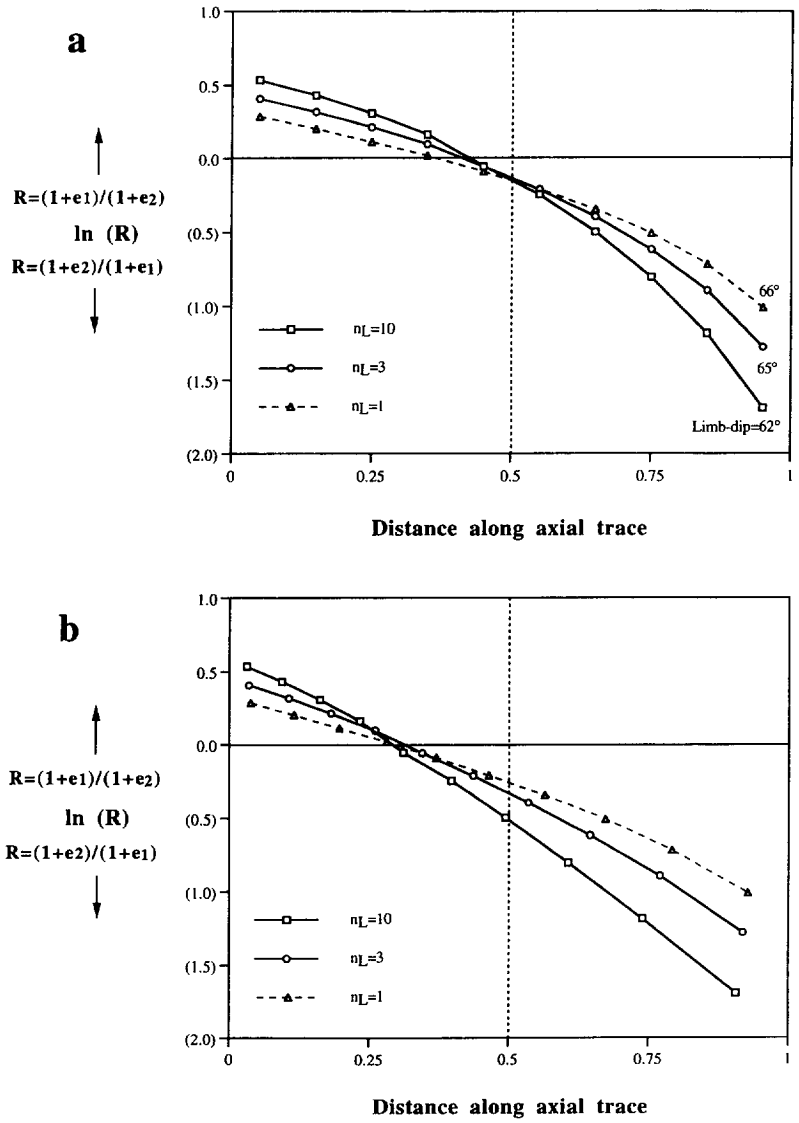

Fig. 7. Strain (expressed as ln R) variation across the stiff layer in the fold hinge from outer arc to inner arc, for $L_o/h_o = 12$, $m = 100$, and $n_L = 1, 3$ and 10. (a) With respect to the unstrained state; (b) with respect to the strained state. The mid point of the layer is shown by the vertical dashed line.

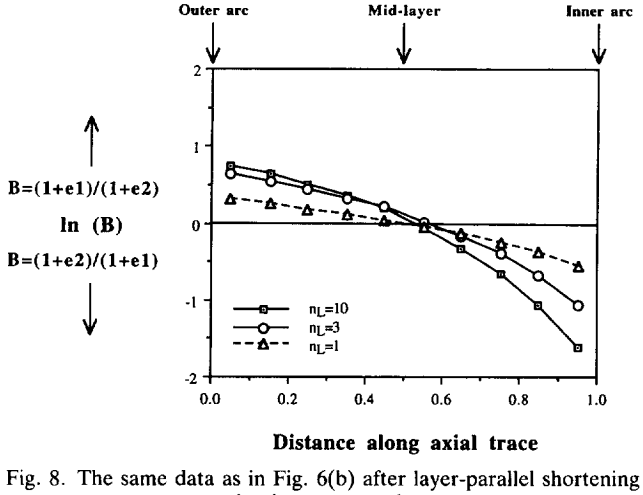

Fig. 8. The same data as in Fig. 6(b) after layer-parallel shortening has been removed.

two neutral surfaces: one in the strain-rate field, the infinitesimal neutral surface (INS), as well as the one in the strain field, the finite neutral surface, at any stage of fold growth (see Ramsay & Huber 1987, pp. 459–461). The position of the two will generally not coincide.

At very low fold amplitudes, during early stages of fold growth, deformation is dominated by layer-parallel shortening (see Fig. 4). The stretch parallel to layering due to buckling, as approximated by the tangential-longitudinal strain model, is a linear function of distance from the neutral surface and curvature of the neutral surface (Ramsay 1967, pp. 397–400). It involves stretching in the outer arc and contraction in the inner arc, and it will increase in magnitude as the fold grows and the curvature increases. The extensional stretch due to buckling is greatest at the outer arc of the stiff layer in the fold hinge, and if the stretching rate at this point grows to become equal to the rate of layer-parallel shortening, the outer-arc hinge point becomes one of zero strain rate—it is an infinitesimal neutral point (Brun 1983). As the fold continues to grow, the rate of stretching in the outer arc of the fold exceeds the rate of layer-parallel shortening and an infinitesimal neutral surface moves down (for anticlines) or up (for synclines) into the layer. Eventually, the buckling-related finite extension at the outer arc in the fold hinge may come to counteract exactly the total layer-parallel shortening, resulting in

zero finite stretch. A 'finite neutral point' will then appear. The finite neutral surface will then move into the layer with continued fold growth. There is thus a shift in position of both neutral surfaces during fold deformation, moving away from the outer arcs into the layer. In sympathy with the movement of the INS and FNS into the layer, there are zones of extensional strain rate and finite extension that move in the opposite direction into the matrix away from the hinges. There is no neutral surface in this case, however, because of the layer-parallel shear strains: instead there are an infinitesimal neutral point and finite neutral point lying in each fold axial surface (see Ramsay & Huber 1987, fig. 21.22).

We have traced the migration of the INS and FNS in the hinges of the folds in the stiff layers of our models for both linear and non-linear cases. The position of the neutral surfaces are found at successive stages of fold growth by interpolation of the strain rate and finite strain values along the axial surface trace of the stiff layer. The results are shown in Fig. 9, and it should be emphasized that the positions of the grid points in each plot of this figure are those in the undeformed state. As anticipated from the discussion above, in all three models (Figs. 9a–c) the INS first appears in the outer arc of the stiff layer, and moves gradually across the layer towards the inner arc. In the two non-linear cases (Figs. 9b & c), the INS appears at an early stage of deformation, and crosses the middle of the layer at about 20% bulk shortening for n_L = 3 and 15% bulk shortening for n_L = 10. In these two cases, the finite neutral surface also first appears early in the experiments and moves down into the layer following the INS. The FNS just about reaches the middle of the layer, again in both cases, at a bulk shortening of 60%. It is also apparent from Fig. 9 that the distance between the INS and the FNS increases as n_L and S (%) increase.

The data shown in Fig. 9 are also plotted in Fig. 10, in which the distance across the layer are now given with reference to the deformed state. Note that in the two non-linear cases (Figs. 10b & c) the INS now reaches the middle of the layer later in the deformation history and the FNS does not reach the middle of the layer.

The situation for the linear model is very different from that for either of the non-linear models (Figs. 9a and 10a). Although the INS moves from the outer edge of the layer towards the center, it does not come into existence until the bulk shortening, S, is 30–35%. Another important difference is that having moved steadily into the layer until about 50% bulk shortening, it abruptly shifts direction and begins to move back towards the outer edge. Note that the FNS never comes into existence: the extensional strain due to buckling does not exceed the large contractional strain due to layer-parallel shortening. This is consistent with the earlier discussion of the strain history of individual nodes (Figs. 5 and 6).

The behavior of the INS in the linear case (Figs. 9a and 10a) can be understood qualitatively in terms of the contribution of buckling to deformation at different stages of fold growth. In the first part of the fold history,

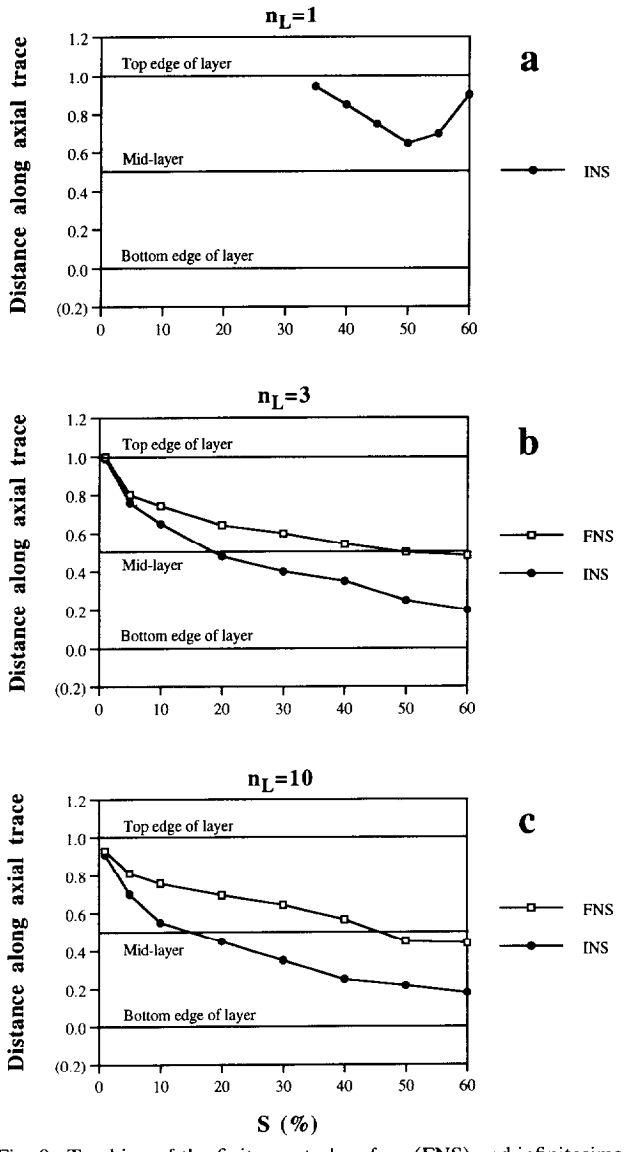

Fig. 9. Tracking of the finite neutral surface (FNS) and infinitesimal neutral surface (INS) along the axial trace as layer-parallel shortening, S, increases, with respect to the undeformed state. For L_o/h_o = 12 and A_o/h_o = 0.1. (a) n_L = 1 and m = 10 (no FNS can be defined); (b) n_L = 3 and m = 215; (c) n_L = 10 and m = 630.

already discussed, layer-parallel shortening exceeds the extensional strains due to buckling until a shortening of about 30%. Buckling is most efficient at intermediate limb dips, reflected by the movement of the INS into the layer. When folds attain high limb dips or become tight, further buckling is resisted by the matrix material between the limbs of the folds, which must be extruded to allow further fold growth (Chapple 1968). Thus a growing proportion of the deformation is taken up by 'flattening' of the folds, a late stage of deformation that is rather uniform. This occurs in our model at S >50% (Figs. 9a and 10a). The return to a relatively more uniform strain-rate field causes the INS to move back towards the outer arc of the fold (Figs. 9a and 10a). (If it were truly uniform, of course, the INS would cease to exist.)

We find that the behavior of the INS and FNS largely depend on the strength of the buckling instability, which depends in turn on both viscosity ratio, m, and on power-law exponent, n_L. Let us consider two cases

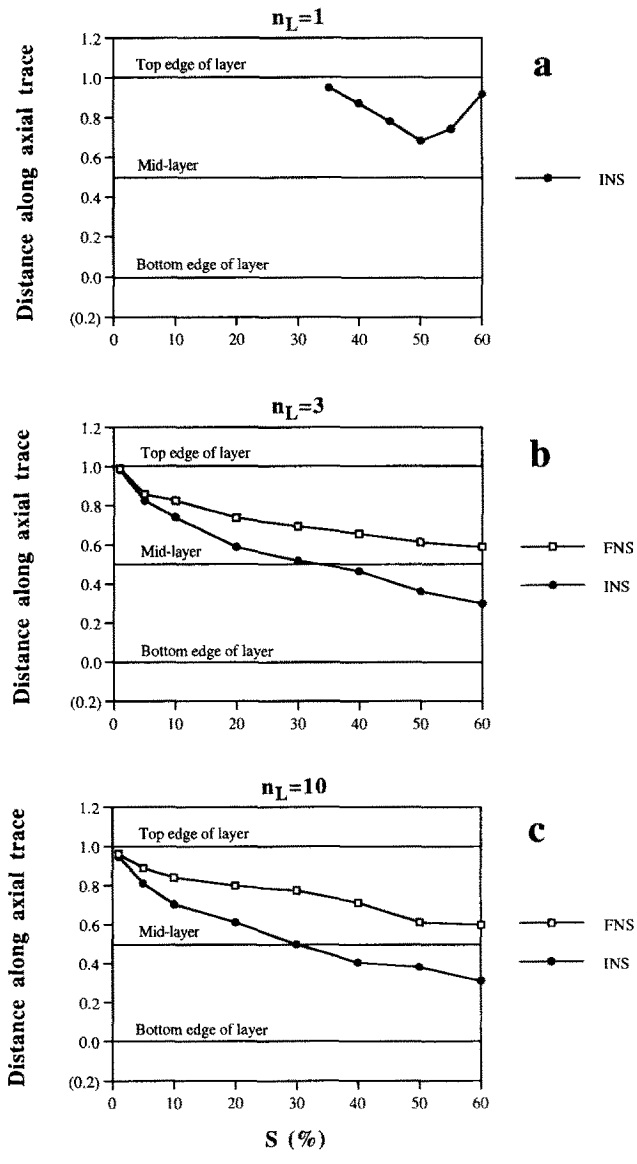

Fig. 10. The same as Fig. 9, plotted with the frame of reference being the deformed state.

intermediate between the range of instabilities represented in Figs. 9 and 10. In a linear case, with $n_L = 1$ and $m = 100$, the instability, being stronger than for $m = 10$, results in the INS appearing much earlier in the deformation history (at about $S = 5\%$) and, unlike the situation for $m = 10$, the FNS exists and appears fairly early in the deformation history (Fig. 11—solid lines, see also Fig. 9). The late stage effect of the INS and FNS beginning to move back towards the outer arc is seen for $m = 100$ (Fig. 11—solid lines), as for $m = 10$, but is not as pronounced. In a non-linear case of roughly comparable instability, with $n_L = 3$ and $m = 43$ (Fig. 11—dashed lines), the development of the INS and FNS is in fact quite similar, except that there is no late-stage shift of the neutral surfaces back towards the outer arc.

The results of tracking the infinitesimal and finite neutral surfaces in all the various models are summarized in Fig. 12. The INS in buckle folds developed in both non-linear and linear materials first appears in the hinge at the outer edge of the stiff layer, and it moves well down across the layer as bulk shortening increases (Fig. 12a), except when the instability is very weak ($n_1 = 1$, $m = 10$). The FNS (Fig. 12b) follows the INS into the layer, except when the instability is so weak ($n_L = 1, m = 10$) that it never comes into existence. It always lies above the INS.

DISCUSSION

The pattern of finite strain in our numerically simulated buckle folds is very close to the theoretical one of tangential longitudinal strain, with layer-parallel extension in the outer arc and contraction in the inner arc (Fig. 3), with the additional effect of an early uniform layer-parallel shortening. This is consistent with earlier numerical models of folding (Dieterich & Carter 1969, Dieterich 1970, Shimamoto & Hara 1976), experiments on folding (Ramberg 1962, 1963b, 1964, Hudleston 1973) and studies on natural folds (Groshong 1975, Hudleston & Holst 1984, Hudleston & Tabor 1988). Field evidence of significant *finite* extension in the outer arcs of natural folds is limited, suggesting that layer-parallel shortening is important in nature. An illustration of the relatively unusual occurrence of finite stretching in the outer arcs of folds is provided by Roberts (1971), who observed what he referred to as an 'abnormal' cleavage pattern in pelitic layers that implied the existence of a finite neutral surface in the folds in adjacent psammitic layers. In about a dozen folds in psammitic layers in pelitic schists studied by Hara *et al.* (1968), about half showed evidence of a finite neutral surface on the basis of the shapes of the quartz grains. Although evidence of finite stretching in outer arcs of fold hinges is not that common, evidence of *incremental* extension, in the form of extensional veins (e.g. Srivastava & Hudleston 1991) or in crystallographic fabric development (Hudleston & Tabor 1988) is widespread.

Our tracking of the INS and FNS during folding indicates that strain history in a buckle fold is not as straight-forward as continuous extension in the outer arc and continuous shortening in the inner arc. We have seen that at any stage of folding there is an INS situated on the inside of the FNS. Thus the stiff layer can be divided into three zones with different, nearly coaxial strain histories at a fixed shortening (Fig. 13). The outer zone (III) has suffered initial contraction and subsequent finite elongation. Between the FNS and INS (zone II) the layer has suffered finite shortening, yet the last part of the history is extensional. Below the INS the layer has undergone continuous shortening. In some cases, where layer-parallel shortening has been large, zone III does not exist and only finite shortening strains are preserved. The division of the layer into zones with different strain histories is implicit in the results of other finite element models of folding (see Dieterich 1969, figs. 2 and 3, Dieterich & Carter 1969, fig. 10, Parrish 1973, fig. 5).

It is interesting to see how the position of the FNS compares with what can be predicted theoretically. Hudleston & Tabor (1988) showed that the position of

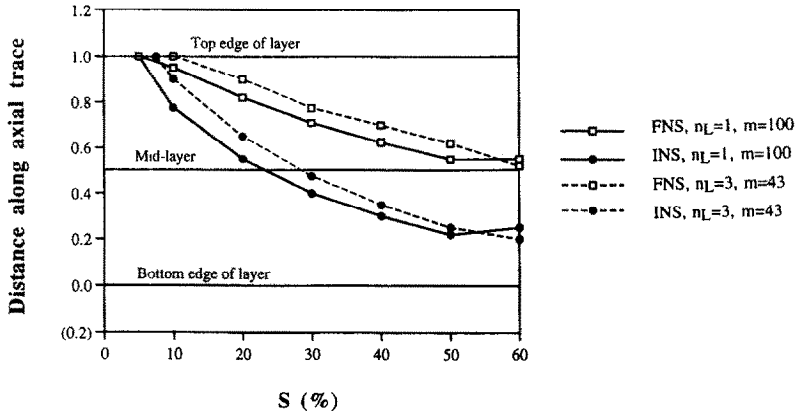

Fig. 11. Similar plot to Fig. 9 for $n_L = 1$, $m = 100$ and $n_L = 3$, $m = 43$. In both cases $L_o/h_o = 12$, $A_o/h_o = 0.1$.

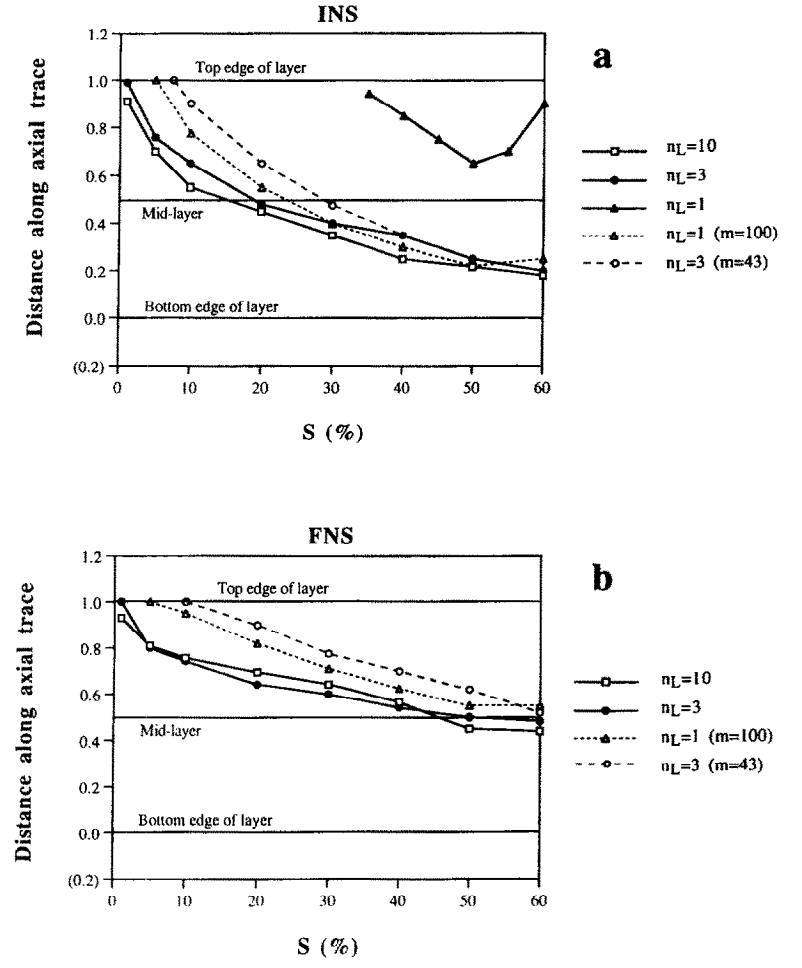

Fig. 12. Comparison of the shift in position of the FNS and INS along the axial trace of the fold with increasing shortening for different sets of rheological parameters. (a) INS and (b) FNS. In all cases $L_o/h_o = 12$, $A_o/h_o = 0.1$.

the neutral surface that minimizes the work done in distorting the layer (assuming that work done is proportional to strain intensity) is at the center of the layer in the deformed state (Hudleston & Tabor 1988, fig. 6). This implies that material lines that were progressively further from the center of the layer towards the inner arc become the neutral surface as a fold grows and as the radius of curvature is decreased. If the theory is correct, the strain at the mid-point of the layer due to buckling alone should be zero ($R = 1$), and thus the strain recorded there, R_m, should be equal to the layer-parallel shortening (T_m) imposed before significant buckling has occurred. The layer-parallel strain can be found independently as discussed in an earlier section, and the error involved in assuming that the strain at the center of the stiff layer at 40% shortening for $m = 100$, and $n_L = 1$, 3 and 10 is equal to the layer-parallel shortening is given in Table 1. Our numerical results are closely consistent with the theoretical prediction for $n_L = 1$ (see Fig. 7b), but deviate significantly from this prediction for $n_L = 3$ and 10. This is to be expected because, for non-linear materials, work done is no longer proportional to strain

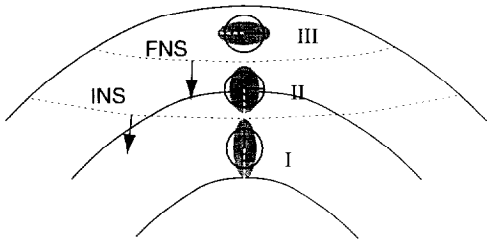

Fig. 13. Schematic diagram to show three zones with different strain histories defined by positions of the infinitesimal neutral surface and finite neutral surface at any instant of folding. Total strains are represented by the shaded ellipses, with the maximum stretch directions shown by the dashed white lines; infinitesimal strains are represented by the solid-line ellipses, with directions of maximum strain rate shown by solid lines.

intensity, because of the strain rate-softening of the flow law. If strain at the center of the stiff layer were used to estimate the bulk strain undergone by the rocks, this would result in an overestimation of 10% for $n_L = 3$ and of 25% for $n_L = 10$.

The strain history of shortening followed by elongation in the stiff layer, of course, is imposed on the material elements of the rocks, and must be accommodated in some way. It might be recorded in many naturally deformed rocks by superimposed small scale structures which apparently 'contradict' each other in the sense that maximum shortening implied by one structure is perpendicular to the maximum shortening implied by another (Ramsay & Huber 1987, pp. 459–462). Likely evidence of extensional and contractional strains in low-grade rocks is vein-filled fractures and pressure solution films, respectively. Neither of these can be simply reversed and removed once formed should the principal deviatoric stresses change. As noted by Ramsay (1967, pp. 114–120), a single tectonic event might result in a complex deformation process with progressively changing geometric constraints, giving the appearance of separate events.

For deformation at higher metamorphic grades, increments of earlier contraction followed by extension may be more difficult to see: crystallographic fabrics resulting from crystal-plastic deformation mechanisms might partially or wholly overprint earlier fabrics (e.g. Lister 1977).

A key question of this project was what differences in internal strain pattern can be attributed to differences in the power-law exponent, n_L? We noted that the strain gradient along the axial trace was more linear for $n_L = 1$ than for $n_L = 3$ and 10 (Figs. 6b, 7b and 8). This is what we would expect from simple beam theory. In simple (thin plate and low-amplitude) buckling, the layer-parallel normal stress varies linearly across the layer and is directly related to curvature (Beer & Johnston 1981). If stress is linearly related to strain rate, a similar distribution of strain will exist in a Newtonian material (some deviation from linearity is to be expected as beam thickness and fold amplitude are increased). If the material is of power-law type (with $n_L > 1$), the strain rate and strain will increase more rapidly away from the neutral surface on both sides than they will in a linear material. Thus the finite strain gradient will be greater for non-linear than for linear materials for a given curvature of the layer. A similar difference between Newtonian and non-Newtonian materials in the gradient of shear strain away from an interface between the two types of material was noted in simple-shear experiments carried out by Treagus & Sokoutis (1992).

Our numerical results show that the finite strain gradient changes systematically with an increase of n_L (Fig. 7). It can be seen from Fig. 7(b) that the strain gradient along the axial trace for models of similar L/h, limb dip and amplitude is greatest for $n_L = 10$ and least for $n_L = 1$. There is a shape difference (Hudleston & Lan 1994) that can be related to this difference in strain gradient—as n_L is increased, the folds become more straight-limbed and sharper hinged, and the gradient of strain along the axial trace is increased. Both strain gradient and shape effects are due to the phenomenon of strain-rate 'softening' in the hinge as n_L is increased. In the non-linear stiff layers in our models strain is concentrated in the fold hinges and is associated with modest early hinge thickening. Strain gradient is a feature that could be established in natural folds, and the gradient compared with the gradients in numerical models of folds of similar L/h, limb dip and amplitude.

Although only in models with $n_L = 1$ did we find the situation in which no FNS developed, it should be pointed out that one cannot consider the lack of a neutral surface in natural folds to be indicative of a linear flow law, because other rheological conditions, such as strain softening or very low viscosity ratio in non-linear flow can produce a similar effect.

By the same token, we cannot conclude that the presence of a FNS indicates non-linear flow. In the linear model with a high viscosity ratio ($m = 100$) and in the non-linear model ($n_L = 3$) with a low viscosity ratio ($m = 43$), both INS and FNS were defined (Fig. 11). For the linear models, a tendency for a later stage compression (with the INS moving back towards the outer arc) exists whatever the viscosity ratio ($10 \leq m \leq 100$ in this study) (Figs. 9a, 10a and 11).

An interesting thing to note in Fig. 12 is that the INS in all models (except for $n_L = 1$, $m = 10$) converge to a similar position in the layer (distance ≈ 0.21, see Fig. 12a) at high values of overall shortening. Likewise, the FNS in all models converge to a position (at about

Table 1. Comparison between theoretical and observed strains at the mid-point of the stiff layer along the fold axial-surface trace, for three models with $m = 100$. R_m is the total strain recorded at the center of the layer in the models, T is the true layer-parallel 'shortening' strain calculated from the change in length of the layer (i.e. the true 'shortening' strain experienced by the system prior to buckling). E is the error, as a percentage, in taking R_m to be the layer-parallel shortening strain

n_L	1	3	10
R_m	1.30	1.40	1.67
T	1.31	1.27	1.25
E%	1	10	25

distance ≈ 0.5, see Fig. 12b) in the middle of the layer. This suggests that the INS and FNS do not move too much as folding reaches the 'flattening stage' (i.e. $S \geq 50\%$). This further suggests that the biggest distinction between folds developed under different conditions of n_L may be made when the folds are of modest amplitude. This is consistent with the results of our earlier study on fold shape (Hudleston & Lan 1990, 1993).

Finally, it is important to note that the deformation in the hinge region of buckle folds formed under conditions of bulk steady-state coaxial flow is not steady state, but is non-linear quasi-coaxial flow, with exchange in principal directions of strain rate and strain possible in the outer arc of the stiff layer (zones II and III in Fig. 13). Even the simplest conditions of bulk strain may give rise to quite complex local effects.

Acknowledgements—This research was supported by the National Science Foundation (EAR-8804670 and EAR-9017922) and the University of Minnesota Supercomputer Institute. We are grateful to Martin Casey, Frederick Vollmer and Susan Treagus for their reviews and suggestions for improvement of the manuscript.

REFERENCES

Beer, F. P. & Johnson, E. R. Jr. 1981. *Mechanics of Materials*. McGraw-Hill, New York.

Biot, M. A., Ode, H. & Roever, W. L. 1961. Experimental verification of the folding of stratified viscoelastic layers. *Bull. geol. Soc. Am.* **72**, 1621–1630.

Brun, J. P. 1983. Isotropic points and lines in strain fields. *J. Struct. Geol.* **5**, 321–327.

Carter, N. L. 1976. Steady state flow of rocks. *Rev. Geophys. Space Phys.* **14**, 301–360.

Chapple, W. M. 1968. A mathematical theory of finite-amplitude rock-folding. *Bull. geol. Soc. Am.* **79**, 47–68.

Chapple, W. M. 1969. Fold shape and rheology: the folding of an isolated viscous-plastic layer. *Tectonophysics* **7**, 97–116.

Cloos, E. 1947. Oolite deformation in the South Mountain Fold, Maryland. *Bull. geol. Soc. Am.* **58**, 843–918.

Dieterich, J. H. 1969. Origin of cleavage in folded rocks. *Am. J. Sci.* **267**, 155–165.

Dieterich, J. H. 1970. Computer experiments on mechanics of finite amplitude folds. *Can. J. Earth Sci.* **7**, 467–476.

Dieterich, J. H. & Carter, N. L. 1969. Stress history of folding. *Am. J. Sci.* **267**, 129–154.

Donath, F. A. & Parker, R. B. 1964. Folds and folding. *Bull. geol. Soc. Am.* **75**, 45–62.

Elliott, D. 1972. Deformation paths in structural geology. *Bull. geol. Soc. Am.* **83**, 2621–2638.

Fletcher, R. C. 1974. Wavelength selection in the folding of a single layer with power-law rheology. *Am. J. Sci.* **274**, 1029–1043.

Fletcher, R. C. 1979. The shape of single-layer folds at small but finite amplitude. *Tectonophysics* **60**, 77–87.

Ghosh, S. K. 1966. Experimental tests of buckling folds in relation to strain ellipsoid in simple shear deformations. *Tectonophysics*, **3**, 169–185.

Ghosh, S. K. 1968. Experimental tests of buckling folds in relation to strain ellipsoid in simple shear deformations. *Tectonophysics* **5**, 343.

Groshong, R. H., Jr. 1975. Strain, fractures, and pressure solution in natural single-layer folds. *Bull. geol. Soc. Am.* **86**, 1363–1376.

Hanson, B. H. 1990. Thermal response of a small ice cap to climatic forcing. *J. Glaciol.* **36**, 49–56.

Hara, I., Uchibayashi, S., Yokota, Y., Umemura, H. & Oda, M. 1968. Geometry and internal structures of flexural folds: (I) Folding of a single competent layer enclosed in thick incompetent layer. *J. Sci. Hiroshima University, Ser. C* **6**, 51–113.

Hobbs, B. E. 1971. The analysis of strain in folded layers. *Tectonophysics* **11**, 329–375.

Holst, T. B. 1987. Analysis of buckle folds from the early Proterozoic of Minnesota. *Am. J. Sci.* **287**, 612–634.

Hudleston, P. J. 1973. An analysis of single layer folds developed experimentally in viscous media. *Tectonophysics* **16**, 189–214.

Hudleston, P. J. & Holst, T. B. 1984. Strain analysis and fold shape in a limestone layer and implications for layer rheology. *Tectonophysics* **106**, 321–347.

Hudleston, P. J. & Lan, L. 1990. The shapes of single-layer folds. *Geol. Soc. of Am. Abs. w. Prog.* **22**, A138.

Hudleston, P. J. & Lan, L. 1993. Information form fold shapes. In: *Special Issue—"Geometry of Naturally Deformed Rocks". J. Struct. Geol.* **15**, 253–264.

Hudleston, P. J. & Lan, L. 1994. Rheological controls on the shapes of single-layer folds. *J. Struct. Geol.* **16**, 1007–1021.

Hudleston, P. J. & Tabor, J. R. 1988. Strain and fabric development in a buckled calcite vein. *Bull. geol. Instn. Univ. Upsala* **14**, 79–94.

Kirby, S. H. & Kronenberg, A. K. 1987. Rheology of the lithosphere: selected topics. *Rev. Geophys.* **23**, 1219–1244.

Lan, L. & Hudleston, P. J. 1991. Finite element models of buckle folds in non-linear materials. *Tectonophysics* **199**, 1–12.

Law, R. D. 1990. Crystallographic fabrics: a selective review of their applications to research in structural geology. In: *Deformation Mechanisms, Rheology and Tectonics* (edited by Knipe, R. J. & Rutter, E. H.). *Spec. Publ. geol. Soc.* **54**, 353–362.

Lister, G. S. 1977. Discussion: Crossed girdle *c*-axis fabrics in quartzites plastically deformed by plane strain and progressive simple shear. *Tectonophysics* **39**, 51–54.

Nicolas, A. & Poirier, J. P. 1976. *Crystalline Plasticity and Solid State Flow in Metamorphic Rocks*. Wiley, London.

Parrish, D. K. 1973. A non-linear finite-element fold model. *Am. J. Sci.* **273**, 318–334.

Paterson, M. S. 1987. Problems in the extrapolation of laboratory rheological data. *Tectonophysics* **133**, 33–43.

Pfiffner, O. A. 1980. Strain analysis in folds (Infrahelvetic complex, Central Alps). *Tectonophysics* **61**, 337–362.

Ramberg, H. 1961. Relationship between concentric longitudinal strain and concentric shearing strain during folding of homogeneous sheets of rocks. *Am. J. Sci.* **259**, 382–390.

Ramberg, H. 1962. Contact strain and folding instability of a multilayered body under compression. *Geol. Rdsch.* **51**, 405–439.

Ramberg, H. 1963a. Evolution of drag folds. *Geol. Mag.* **100**, 97–106.

Ramberg, H. 1963b. Strain distribution and geometry of folds. *Bull. geol. Instn. Univ. Upsala* **42**, 1–20.

Ramberg, H. 1964. Selective buckling of composite layers with contrasted rheological properties, a theory for simultaneous formation of several orders of folds. *Tectonophysics* **1**, 307–341.

Ramsay, J. G. 1967. *Folding and Fracturing of Rocks*. McGraw-Hill, New York.

Ramsay, J. G. & Huber, M. I. 1987. *The Techniques of Modern Structural Geology, Vol. 2, Folds and Fractures*. Academic Press, London.

Roberts, D. 1971. Abnormal cleavage patterns in fold hinge zones from Varanger peninsula, northern Norway. *Am. J. Sci.* **271**, 170–180.

Sherwin, J. & Chapple, W. M. 1968. Wavelengths of single-layer folds: a comparison between theory and observations. *Am. J. Sci.* **266**, 167–179.

Shimamoto, T. & Hara, I. 1976. Geometry and strain distribution of single-layer folds. *Tectonophysics* **30**, 1–34.

Simpson, C. & Schmid, S. M. 1983. An evaluation of criteria to deduce the sense of movement in sheared rocks. *Bull. geol. Soc. Am.* **94**, 1281–1288.

Srivastava, H. B. & Hudleston, P. J. 1991. Experimental development of single-layer buckle folds in non-linear materials. *EOS* **72**, 472.

Treagus, S. H. & Sokoutis, D. 1992. Laboratory modelling of strain variation across rheological boundaries. *J. Struct. Geol.* **14**, 405–424.